Physics and Control of ELMing H–mode Negative Central Shear Advanced Tokamak Scenario Based on Experimental Profiles for ITER

L.L. Lao,[1] V.S. Chan,[1] M.S. Chu,[1] T. Evans,[1] D.A. Humphreys,[1] J.A. Leuer,[1]
M.A. Mahdavi,[1] T.W. Petrie,[1] P.B. Snyder,[1] H.E. St.John,[1] G.M. Staebler,[1]
R.D. Stambaugh,[1] T.S. Taylor,[1] A.D. Turnbull,[1] W.P. West,[1] and D.P. Brennan[2]

[1]General Atomics, P.O. Box 85608, San Diego, California 92186-5608
email: lao@fusion.gat.com
[2]Oak Ridge Institute of Science Education, Oak Ridge, Tennessee.

Abstract. Key DIII–D AT experimental and modeling results are applied to examine the physics and control issues for ITER to operate in a negative central shear (NCS) AT scenario. The effects of a finite edge pressure pedestal and current density are included based on the DIII-D experimental profiles. Ideal and resistive stability analyses indicate that feedback control of resistive wall modes by rotational drive or flux conserving intelligent coils is crucial for these AT configurations to operate at attractive β_N values in the range of 3.0–3.5. Vertical stability and halo current analyses show that reliable disruption mitigation is essential and mitigation control using an impurity gas can significantly reduce the local mechanical stress to an acceptable level. Core transport and turbulence analyses demonstrate that control of the rotational shear profile is essential to maintain the good confinement necessary for high β. Consideration of edge stability and core transport suggests that a sufficiently wide pedestal is necessary for the projected fusion performance. Heat flux analyses indicate that with core-only radiation enhancement the outboard peak divertor heat load is near the design limit of 10 MW/m^2.

1. Introduction and Overview

The goal of magnetic fusion research is to develop fusion energy as an economical and viable energy source. Two of the major research elements are the development of advanced tokamak (AT) configurations with good confinement and improved stability at high β and steady-state, and the study of these configurations under burning plasma conditions. An international fusion energy advanced tokamak burning plasma machine, ITER-FEAT [1], has recently been proposed to study inductive and steady-state burning plasmas, which offers an opportunity to continue development of the AT path.

In this paper, the potential for ITER-FEAT to operate in an ELMy H-mode AT scenario is evaluated. The study also provides an opportunity to identify crucial AT research and development issues necessary to advance ITER. Using the ITER-FEAT inductive and steady state advanced reference scenarios [2] as starting points, key DIII–D AT experimental and modeling results are applied to assess the requirements for ITER-FEAT to operate in an ELMing H–mode negative central shear (NCS) AT scenario. These include rotation and feedback stabilization of resistive wall modes (RWMs) for high β operation, constraints on core transport and the edge pedestal for high fusion performance due to drift-wave based transport and ELMs, disruption mitigation, and divertor heat load. The effects of a finite edge pressure pedestal and current density are included based on representative experimental pressure and current profiles from recent DIII-D long-pulse high performance discharges.

2. MHD Equilibrium

Two key features of H-mode discharges are the finite edge pressure pedestal and the associated edge bootstrap current. In this study, the MHD equilibria are computed based on representative current and pressure profiles taken from recent DIII–D long-pulse high-performance AT discharges with realistic edge density and temperature pedestals.

The flux-surface averaged toroidal current density $\langle J_\phi \rangle$ and the pressure gradient $P'(\psi)$ for these DIII-D like AT equilibria are distinguished by their finite edge pedestals. These are illustrated in Figs. 1(a) for a base equilibrium. The pressure P and the safety factor q profiles are given in Fig. 2(a). The global plasma parameters for this base case are compared to those of the ITER-FEAT inductive and steady-state AT reference configurations [2] in Table I. Also shown for comparison in Table I are the corresponding parameters for a JT-60U AT discharge [3].

3. Power Balance and Energy Confinement

One of the key ITER-FEAT physics questions is whether its energy confinement is sufficient to allow it to study long pulse high β and high confinement AT physics issues. Power balance analyses using the ONETWO branch of the Corsica transport module indicate that values of $H_{89P} \geq 2.4$ are necessary to operate at values of $\beta_N \sim 3.0$–3.5. This is summarized in Table II, where the energy confinement required to obtain $\beta_N \sim 3.1$ with various amounts of neutral beam and rf auxiliary heating power are compared. In these calculations, $\langle n_e \rangle \sim 0.93\, n_{GW}$. The n_i profile used in the calculations is taken from representative DIII-D AT experimental discharges. The ion and electron temperature T_i and T_e profiles are obtained from the equilibrium P and the density profiles and are taken to be equal. They are given in Fig. 2(b). These parameters are similar to those given in Ref. [4], although the plasma volume, I_P, $B\phi_0$, and fusion power are larger and $\langle Z_{eff} \rangle$ is smaller.

4. Pressure-Driven Ideal and Resistive MHD Stability

Two of the major issues for AT operations are the stability against the pressure-driven MHD modes and the stabilization of these modes. DIII-D experimental results show that wall stabilization plays an important role in the high β discharges and $n = 1$ RWMs are the dominant MHD instabilities. DIII-D experimental results also suggest that plasma toroidal rotation and external coil feedback are effective for stabilization against these modes [5].

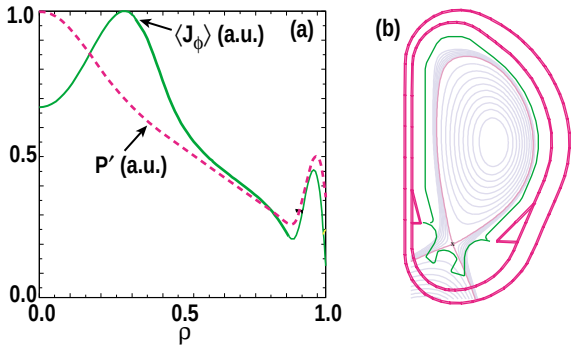

Fig. 1. (a) Flux-surface averaged toroidal current density $\langle J_\phi \rangle$ and pressure gradient $P'(\psi)$ and (b) flux surfaces for the DIII-D AT-like base equilibrium.

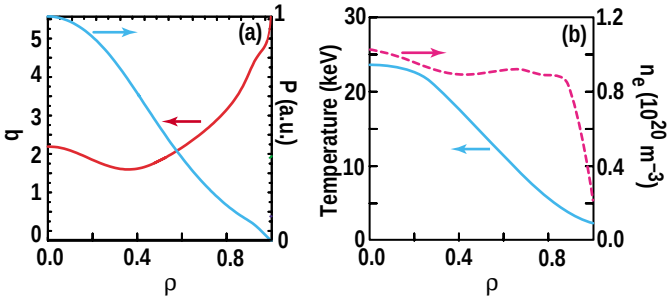

Fig. 2. Radial profiles of (a) pressure P and safety factor q, (b) temperature and density profiles for the DIII-D like AT base equilibrium. T_i is taken to be equal to T_e.

TABLE I: Comparison of ITER-FEAT Major Plasma Parameters for Three Different Scenarios. Also Shown are the Parameters for a JT-60U AT Discharge.

Case	Inductive [2]	Steady State [2]	DIII-D AT-Like	JT-60U [3]
I_p (MA)	15	10	10	1.5
B_T (T)	5.3	5.3	5.3	3.6
R (m)	6.20	6.35	6.35	3.30
a (m)	2.0	1.85	1.86	0.82
κ_x	1.85	1.95	1.94	1.48
δ_x	0.49	0.56	0.52	0.36
q_0	1.0	2.4	2.2	1.90
q_{min}	1.0	2.0	1.6	1.75
q_{95}	3.0	4.4	4.7	4.1
β_N	1.8	3.2	3.3	2.8
β_p	0.65	1.80	1.90	1.97
β_T(%)	2.5	3.3	3.4	1.43
ℓ_i	0.85	0.67	0.56	0.78

Ideal stability analyses indicate that these DIII-D-like AT equilibria with $\beta_N \sim 3.0$–3.5 are unstable to the ideal $n = 1$–3 modes without a conducting wall. They are stable with a wall at 1.2 times the actual ITER-FEAT wall, r_{ITER}. The β limit against the $n = 1$ modes without a conducting wall is $\beta_N \sim 2.1$. With a conducting wall at r_{ITER}, it is stable up to $\beta_N \sim 5.5$. With low edge current density, the no-wall limit is increased to $\beta_N \sim 2.5$. For operation at values of $\beta_N > 2.1$, it is therefore important to maintain the stability against these pressure-driven kink modes.With increased triangularity δ, the n=2 and 3 modes become stable even without a wall.

TABLE II: Comparison of ITER-FEAT Fusion Gain and Required Energy Confinement Enhancement Factor for Three Amounts of Input Power.

Case	None	Beam	Beam + RF
$\langle n_e \rangle$ (10^{20}m^{-3})	0.85	0.85	0.85
$\langle T \rangle$ (keV)	10.7	10.7	10.7
$\langle Z_{eff} \rangle$	1.8	1.8	1.8
P_{BEAM} (MW)	0	33	33
P_{RF} (MW)	0	0	66
Q	∞	20	6.7
β_N	3.0	3.1	3.1
β_T(%)	3.1	3.2	3.2
τ_E (s)	2.9	2.4	1.7
H_{89P}	3.1	2.8	2.4
P_{FUSION} (MW)	660	660	660
T^{PED} (keV)	4	4	4
F_{BS} + F_{NNBI} (%)	47	66	66

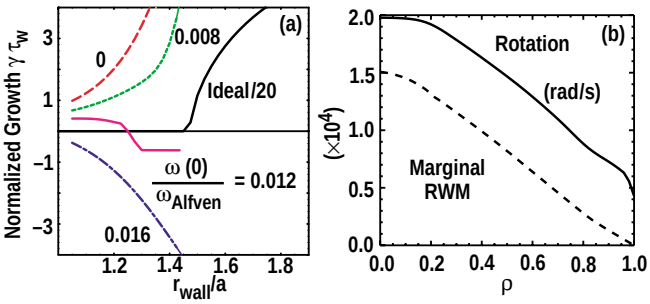

Fig. 3. (a) Variation of the n=1 RWM growth rate γ normalized to the resistive wall time τ_W at various central rotation frequency as a function of the distance to the wall. (b) Toroidal rotation profile (solid curve) produced using 33 MW of 1 MeV tangential NNBI. Also shown is the rotational profile marginally stable to RWM (dashed curve).

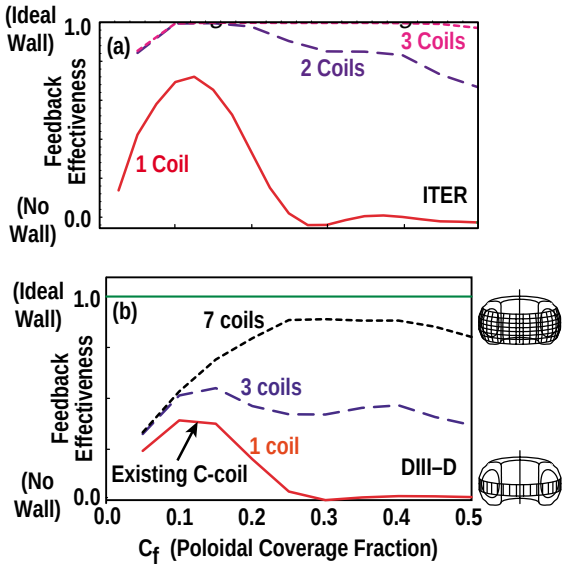

Fig. 4. Variation of feedback effectiveness with poloidal coverage fraction C_f, using various numbers of feedback coils (a) ITER-FEAT, (b) DIII-D. Also shown in Fig. 4(b) are the physical locations of the feedback coils used in the DIII-D calculations.

RWM stability analysis using the MARS code and a sound wave damping model [6,7] indicate that a central rotation rate ~1% of the Alfvén rotation frequency is sufficient to stabilize these *n*=1 RWMs. This is illustrated in Fig. 3(a). The required neutral beam injection power is estimated using ONETWO. The results indicate that ~33 MW of 1 MeV tangential NNBI is needed to provide sufficient rotational drive for stabilization against these *n*=1 RWMs at $\langle n_e \rangle \sim 0.93\, n_{GW}$. This is shown in Fig. 3(b). Temperature and density profiles shown in Section 3 [Fig 2(b)] were used in this analysis and correspond to $H_{89P} \sim 2.8$.

External coil feedback stabilization analyses using a flux-conserving intelligent coil scheme [5] indicate that external coil feedback can also provide an effective means to stabilize the *n*=1 RWMs. This is illustrated in Fig. 4(a). Similar calculations for a DIII-D AT configuration are shown in Fig. 4(b). The calculations are done with an extended energy principle using the GATO and the VACUUM codes [8]. The plasma is assumed to be surrounded by a thin resistive shell and a network of flux conserving coils located at $r_{wall} \sim 1.4a \sim 1.2\, r_{ITER}$. As shown in Fig. 4(a), with a sufficient number of feedback coils, the plasma can be operated near the β limit with a conducting wall.

5. Disruption Mitigation and Halo Current

The poloidal halo current induced during a disruption event can interact with the toroidal magnetic field to produce large local mechanical stress. Recent DIII-D experimental results suggest that controlled plasma termination using high-pressure noble gas-jet injection can significantly reduce the halo current and lower the mechanical stress [9].

Vertical instability and the resulting halo current expected for ITER-FEAT AT configuration are analyzed using the stability package of the CalTrans code and an analytic halo current

model [10]. The results of the analyses indicate that reliable disruption mitigation is crucial for ITER-FEAT, and mitigation using an impurity gas such as Ar can reduce the peaked halo current to an acceptable level. With an Ar gas puff, the peak halo current is reduced from 0.11 to 0.06 I_p and the mechanical stress from 0.47 MPa to 0.12 MPa.

6. Core Transport and Turbulence

One of the key ITER-FEAT issues is whether its energy confinement is sufficient to allow attainment of projected performance. Experimental results from DIII-D and other tokamaks suggest that drift-wave turbulence plays a key role in core energy transport [11]. Drift-wave based transport models such as GLF23 [12] can reasonably predict core temperature profiles.

Transport analysis using the ONETWO code with the recently re-normalized drift-wave based transport model GLF23 [13] indicates that the temperature at the top of the edge pedestal is important in determining the overall fusion performance, as expected. This is illustrated in Fig. 5 where Q ~ 10–15, H_{89P} ~ 2.4–3.0 is achieved at n_e ~ 0.93 n_{GW} with an edge pedestal temperature of ~5–6 keV. To reduce the pedestal temperature requirement, control of rotational drive to stabilize the drift-wave turbulence is essential.

7. Edge Stability, ELM, and Divertor Heat Flux Issues

Evaluation of the effects of ELMs on edge pedestal and divertor heat load is an important ITER-FEAT issue. Experimental and modeling results from DIII-D and other tokamaks support a model of ELMs as ideal, intermediate to high *n* peeling-ballooning modes driven by the steep edge pressure gradient and current density [14,15].

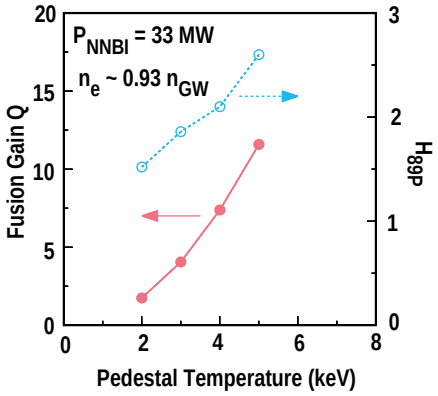

Fig. 5. Variation of fusion gain Q and H_{89P} with pedestal temperature computed using the renormalized GLF23 drift-wave based transport model.

The constraints on the edge pedestal height and the divertor heat load due to ELMs are evaluated by analyzing the edge stability of these configurations against these *n*=10–30 peeling-ballooning modes using the ELITE code [15]. The results indicate that a pedestal width in the range of ~5%–8% ψ_N is needed to reach a pedestal temperature ~5 keV. This is illustrated in Fig. 6, where the maximum pedestal temperature stable to these MHD modes at various edge pedestal widths for three different densities are compared. The calculations are done by super-imposing various edge hyperbolic tangent shaped density and temperature pedestals of equal widths on a generic ITER-FEAT equilibrium. The edge bootstrap current driven by these profiles is self-consistently included using a bootstrap current model.

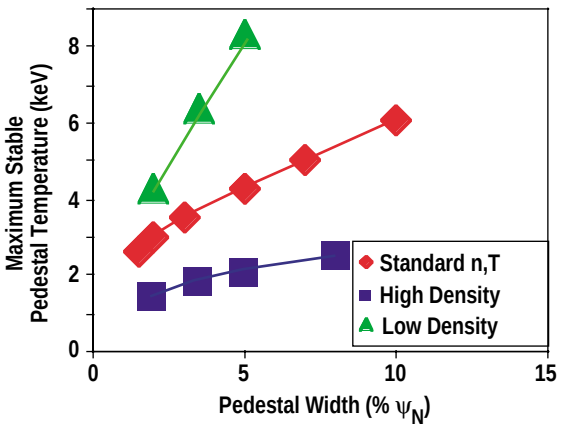

Fig. 6. Variation of the maximum stable pedestal temperature with pedestal width at three different densities computed using the ELITE code.

The prospects of reducing the power flowing into the scrape-off layer (SOL) by radi-

ating a significant fraction of the heating power from inside the main plasma are also evaluated. Two recycling impurities Ar and Kr are considered. The peak heat flux at the outboard divertor target $Q_\perp$ is estimated by assuming the radial heat flux distribution is toroidally symmetric and decays exponentially away from the divertor strike point. The results indicate that $Q_\perp$ is near the design limit of 10 MW/m^2 at $\langle n_e \rangle \sim 0.93\ n_{GW}$ and $\langle Z_{eff} \rangle \sim 1.8$. These analyses are summarized in Table III. Radiation from the SOL and divertor are assumed to make negligible contributions to the radiated power. It may be necessary to operate the divertor in a near-detached condition to further reduce the peak heat flux to a more manageable level.

TABLE III: Comparison of the Peak Heat Flux at the Divertor Target $Q_\perp$ for Ar and Kr.

Z_{eff}	1.8	2.4
Ar $Q_\perp$ (MW/m^2)	12.6	10.1
Ar P_{RAD}(MW)	23.3	45.1
Kr $Q_\perp$ (MW/m^2)	10.6	6.3
Kr P_{RAD} (MW)	39.0	75.9

8. Discussion and Summary

In this paper, various key physics and control issues related to ITER-FEAT AT operations are evaluated based on DIII-D AT experimental and simulation results. These include stabilization of RWMs by rotational drive or external coil feedback, disruption mitigation, constraint on edge pedestal width due to ELMs and core turbulence, and divertor heat load.

The results suggest that feedback control of resistive wall modes by rotational drive or flux conserving intelligent coils are crucial for these AT configurations to operate at β_N values of 3.0–3.5. Reliable disruption mitigation is necessary to reduce the local mechanical stress to an acceptable level. Control of the rotational shear profile is also essential to maintain good confinement necessary for high β. A sufficiently wide pedestal is necessary for the projected fusion performance. Core-only radiation may be marginal to reduce the peak divertor heat load to a tolerable level.

Acknowledgment

The work discussed in this paper was supported by General Atomics Internal Research and Development Funds, the US Department of Energy under Contracts DE-AC03-99ER54463 and DE-AC05-76OR00033.

References

[1] R. Aymar, *et al.*, Nucl. Fusion **41**, 1301 (2001).
[2] Y. Gribov, *et al.*, in Fusion Energy 2000 (Proc. 17th Int. Conf., Sorrento, 2000) IAEA, Vienna (2001) Paper ITERP/02.
[3] Y. Kamada, *et al.*, Fusion Energy 1996 (Proc. 16th Int. Conf., Montreal, 1996) Vol. 1, IAEA, Vienna (1997) 227.
[4] Y. Shimomura, *et al.*, Nucl. Fusion **41**, 309 (2001).
[5] A.M. Garofalo, *et al.*, Phys. Plasmas **9**, 1997 (2002).
[6] A. Bonderson, *et al.*, Phys. Fluids **B4**, 1889 (1992).
[7] M.S. Chu, *et al.*, Phys. Plasmas **2**, 2236 (1995).
[8] M.S. Chance., *et al.*, Nucl. Fusion **42**, 295 (2002).
[9] D.G. Whyte, *et al.*, Phys. Rev. Lett. **89**, 055001 (2002).
[10] D.A. Humphreys, *et al.*, Phys. Plasmas **6**, 2742 (1999).
[11] K.H. Burrell, *et al.*, Phys. Plasmas **4**, 1499 (1997).
[12] R.E. Waltz, *et al.*, Phys. Plasmas **4**, 2482 (1997).
[13] J.E. Kinsey, *et al.*, this conference.
[14] L.L. Lao, *et al.*, Nucl. Fusion **41**, 295 (2001).
[15] P.B. Snyder, *et al.*, Phys. Plasmas **9**, 2037 (2002).